

Diffusing to Coordinate: Efficient Online Multi-Agent Diffusion Policies

Zhuoran Li^a, Hai Zhong^a, Xun Wang^a, Qingxin Xia^b, Lihua Zhang^b, and Longbo Huang^a

^aInstitute for Interdisciplinary Information Sciences (IIIS), Tsinghua University

^bByteDance

Abstract

Online Multi-Agent Reinforcement Learning (MARL) is a prominent framework for efficient agent coordination. Crucially, enhancing policy expressiveness is pivotal for achieving superior performance. Diffusion-based generative models are well-positioned to meet this demand, having demonstrated remarkable expressiveness and multimodal representation in image generation and offline settings. Yet, their potential in online MARL remains largely under-explored. A major obstacle is that the intractable likelihoods of diffusion models impede entropy-based exploration and coordination. To tackle this challenge, we propose among the first Online off-policy MARL framework using Diffusion policies (**OMAD**) to orchestrate coordination. Our key innovation is a relaxed policy objective that maximizes scaled joint entropy, facilitating effective exploration without relying on tractable likelihood. Complementing this, within the centralized training with decentralized execution (CTDE) paradigm, we employ a joint distributional value function to optimize decentralized diffusion policies. It leverages tractable entropy-augmented targets to guide the simultaneous updates of diffusion policies, thereby ensuring stable coordination. Extensive evaluations on MPE and MAMuJoCo establish our method as the new state-of-the-art across 10 diverse tasks, demonstrating a remarkable $2.5\times$ to $5\times$ improvement in sample efficiency.

Keywords: Diffusion Policy, Multi-Agent Reinforcement Learning

1 Introduction

Multi-agent reinforcement learning (MARL [44]) provides a robust framework for decision-making in complex systems, ranging from autonomous driving [75] to robot swarms [10]. A central challenge in these domains is agent coordination under severe non-stationarity [59]. To mitigate this issue, Centralized Training with Decentralized Execution (CTDE) [5, 50] has emerged as the predominant

paradigm and has achieved remarkable success. However, the prevailing use of unimodal policy distributions (e.g., Gaussian) struggles to represent the highly complex and multimodal coordination strategies [61, 41], which is essential for multi-agent interactions.

In order to address the limitations of policy expressiveness, diffusion-based generative models [23] have emerged as a powerful alternative. Through progressive denoising, diffusion models demonstrate exceptional capability in modeling highly multimodal distributions [56]. This strong expressiveness naturally makes them particularly appealing for sequential decision-making [27, 63], where optimal policies often involve diverse strategies. Indeed, diffusion policies have demonstrated strong performance in offline single- and multi-agent settings with expert demonstrations, achieving substantial gains in manipulation and locomotion tasks [35, 13, 25].

In order to address the limitations of policy expressiveness, diffusion-based generative models [23] have emerged as a powerful alternative. Through progressive denoising, diffusion models demonstrate exceptional capability in modeling highly multimodal distributions [56]. This strong expressiveness naturally makes them particularly appealing for sequential decision-making [27, 63], where optimal policies often involve diverse strategies. Indeed, diffusion policies have demonstrated strong performance in offline single- and multi-agent settings with expert demonstrations, achieving substantial gains in manipulation and locomotion tasks [35, 13, 25].

However, extending diffusion models to online MARL remains challenging, particularly in achieving efficient training from scratch without relying on offline demonstrations. Specifically, the intractable likelihoods [23] inherent in diffusion models hinder efficient exploration. This intractability precludes conventional entropy regularization [20]. Such incompatibility is severely exacerbated in multi-agent settings where coordinated exploration is essential to navigate non-stationarity and discover cooperative strategies [36]. While single-agent adaptations exist [41, 8], extending these frameworks to off-policy MARL remains a non-trivial endeavor.

We tackle these challenges by proposing the first Online off-policy MARL framework tailored for Diffusion policies called **OMAD**. Our algorithm pioneers a tractable maximum entropy paradigm for multi-agent diffusion policies. We break the computational barriers of prior generative MARL approaches by introducing a tractable relaxed joint policy objective. Under this unified framework, we orchestrate a holistic optimization process: training a centralized distributional critic to capture aleatoric uncertainty, guiding per-agent diffusion policies via synchronized updates, and auto-tuning temperature constraints. Facilitating the high expressiveness of diffusion policies, our framework empowers agents to achieve consistent coordination, setting a robust and scalable standard for online generative MARL.

We summarize our key contributions as follows:

- We propose the first online off-policy diffusion framework for MARL. To overcome the intractability of likelihood computation, we introduce a relaxed objective based on scaled joint entropy. This formulation extends tractable exploration to the multi-agent domain, enabling

agents to effectively coordinate their exploration in high-dimensional joint action spaces.

- We develop a unified off-policy learning mechanism within the CTDE paradigm. By leveraging a joint distributional value function, we optimize distinct policies for all agents simultaneously under a single unified objective. This synchronous update strategy effectively mitigates non-stationarity, fostering efficient collaboration and stable convergence.
- We evaluate our **OMAD** algorithm on standard continuous control benchmarks, including Multi-Agent Particle Environments (MPE) and Multi-Agent MuJoCo (MAMuJoCo). Our method establishes a new state-of-the-art across 10 diverse scenarios, consistently surpassing baselines with a substantial $2.5\times$ to $5\times$ gain in sample efficiency.

2 Related Works

Here we highlight key works on online MARL and diffusion policies in RL. A comprehensive discussion is provided in Appendix A.

2.1 Online Multi-Agent Reinforcement Learning

Online multi-agent reinforcement learning (MARL) has made substantial progress under the centralized training with decentralized execution (CTDE) paradigm [44, 50]. Representative methods such as MADDPG [37], MAPPO [69], COMA [18], and value decomposition approaches including VDN [57], QMIX [50], and QPLEX [60] significantly improve coordination and learning stability in cooperative tasks. More recent works focus on addressing non-stationarity, exploration efficiency, and agent heterogeneity, including RES-QMIX [45], SMPE [30] and RCO [34]. In particular, heterogeneity-aware frameworks such as HARL and its variants [74, 36] represent the state of the art by explicitly coordinating heterogeneous agents. Despite these advances, existing online MARL methods predominantly rely on unimodal policy representations, limiting their ability to model complex, multi-modal coordination behaviors.

2.2 Diffusion Policies in Reinforcement Learning

Diffusion models are powerful generative models with strong capacity for representing expressive and multi-modal distributions [23, 56], and have been widely adopted in sequential decision-making, particularly in imitation learning [65] and offline reinforcement learning [63]. Representative approaches such as Diffuser [27], Decision Diffuser [2], and Diff-QL [63] achieve significant gains by modeling complex action or trajectory distributions, with extensions to offline multi-agent settings improving policy diversity [35] and data efficiency [76, 32].

In contrast, extending diffusion policies to online reinforcement learning remains challenging due to intractable likelihoods and inefficient exploration. Recent methods mitigate these issues via value-guided [48, 61] or entropy-regularized objectives [8, 41], but are largely limited to single-

agent settings and do not scale to multi-agent systems with coordinated exploration and non-stationarity. Our work bridges this gap by proposing among the first online off-policy diffusion frameworks tailored for MARL.

3 Preliminary

3.1 MARL and Efficient Value Estimation

We study cooperative multi-agent reinforcement learning in the framework of decentralized partially observable Markov decision processes (Dec-POMDPs) [43]. An N -agent cooperative task is represented by the tuple $G = \langle \mathcal{I}, \mathcal{S}, \mathcal{O}, \mathcal{A}, \Pi, \mathcal{P}, \mathcal{R}, N, \gamma \rangle$. Here, $\mathcal{I} = \{1, \dots, N\}$ denotes the agents, \mathcal{S} is the global state space, $\mathcal{O} = (\mathcal{O}_1, \dots, \mathcal{O}_N)$ represents the local observations, and $\mathcal{A} = (\mathcal{A}_1, \dots, \mathcal{A}_N)$ means the joint action space. Each agent i selects $a_i \in \mathcal{A}_i$ according to its policy $\pi_i \in \Pi_i$. The environment evolves via $\mathcal{P}(s' | s, a)$, and agents receive rewards from the shared function $\mathcal{R} : \mathcal{S} \times \mathcal{A} \rightarrow \mathbb{R}$. The goal of standard MARL is to learn a joint policy $\boldsymbol{\pi} = (\pi_1, \dots, \pi_N)$ maximizing the expected discounted team return $\mathbb{E}_{\boldsymbol{\pi}}[\sum_{t=0}^{\infty} \gamma^t r_t]$, given the discounted factor $\gamma \in [0, 1)$ and the sum of rewards for each agent $r_t = \sum_{i=1}^N r_i^t$.

To prevent premature convergence to sub-optimal deterministic policies in complex multi-agent interactions [36], *Maximum Entropy RL* framework [77, 21] augments the standard return with policy entropy to promote exploration. In multi-agent settings, this translates to maximizing the expected return alongside the joint policy entropy $\mathcal{H}(\boldsymbol{\pi}(\cdot | s_t))$ that: $\mathbb{E}_{\boldsymbol{\pi}}[\sum_{t=0}^{\infty} \gamma^t r_t + \alpha \mathcal{H}(\boldsymbol{\pi}(\cdot | s_t))]$, where α regulates the exploration-exploitation trade-off. For decentralized policies $\boldsymbol{\pi}(\mathbf{a} | s) = \prod_i \pi_i(a_i | s)$ [74], the framework yields a softened Bellman operator, where the soft Q-function is optimized via the Bellman residual:

$$\mathcal{L}_Q(\theta) = \mathbb{E}_{(s, a, r, s') \sim \mathcal{D}} \left[\left(Q_{\theta}(s, a) - \gamma \left(r + Q^{\pi}(s', a') - \alpha \sum_{i=1}^N \log \pi_i(a'_i | s') \right) \right)^2 \right], \quad (1)$$

and the associated soft policy iteration admits the closed-form policy improvement update:

$$\pi_{k+1} = \arg \min_{\pi} D_{\text{KL}} \left(\pi(\cdot | s) \parallel \frac{\exp(\frac{1}{\alpha} Q^{\pi_k}(s, \cdot))}{Z(s)} \right), \quad (2)$$

where $Z(s) = \int \exp(\frac{1}{\alpha} Q^{\pi_k}(s, a')) da'$ is the normalizing factor that does not affect policy optimization.

To ensure reliable value estimation, we list two complementary techniques: CrossQ and Distributional Q-learning. CrossQ [6] eliminates target networks by applying Batch Normalization to concatenated state-action pairs and applying a stop-gradient to the next-state estimates for high update-to-data ratios. Distributional Q-learning [4] models the full return distribution $Z_{\phi}(s, a)$ rather than its expectation $Q_{\phi}(s, a) = \mathbb{E}[Z_{\phi}(s, a)]$ as higher-order return statistics to provide richer

signals, mitigating the high variance of value functions.

3.2 Diffusion policy

Diffusion policy [41, 16, 62, 8] parameterizes the policy as the terminal distribution of a state-conditioned process, governed by continuous-time Ornstein–Uhlenbeck [52] (OU) dynamics over state s and $t \in [0, T]$,

$$da_t = -\beta_t a_t dt + \eta \sqrt{2\beta_t} dB_t, a_0 \sim \pi_0(\cdot|s). \quad (3)$$

Here, β_t and η are diffusion and drift coefficients, B_t is standard Brownian motion, and π_0 is the target policy. Let π_t denote the marginal at time t ; with a proper schedule, this distribution converges to $\pi_T \approx \mathcal{N}(0, \eta^2 I)$. Denoising diffusion policy is defined by the reverse dynamics (Eq. 4) starting from $a_T \sim \mathcal{N}(0, \eta^2 I)$, where a network f_θ approximates the score $\nabla_{a_t} \log \pi_t$ for denoising,

$$da_t = (-\beta_t a_t - 2\eta^2 \beta_t f_\theta(a_t, s, t)) dt + \eta \sqrt{2\beta_t} d\tilde{B}_t. \quad (4)$$

This yields samples $a_0 \sim \pi_\theta$. Theoretically, accurate score estimation $f_\theta \approx \nabla \log \pi_t$ ensures π_θ recovers the target π_0 . Applying Euler-Maruyama discretization [52], the discrete forward and reverse dynamics are:

$$a_{h+1} = a_h - \beta_h a_h \delta + \epsilon_h, \quad (5)$$

$$a_{h-1} = a_h + (\beta_h a_h + 2\eta^2 \beta_h f_\theta(a_h, s, hT/H)) \delta + \xi_h. \quad (6)$$

Here, $\epsilon_h, \xi_h \sim \mathcal{N}(0, 2\eta^2 \beta_h \delta I)$, step size $\delta = T/H$, and $a_h \equiv a_{th/T}$. Under EM discretization, the noising and denoising processes exhibit the following joint distributions:

$$\pi(a_{0:H}|s) = \pi(a_0|s) \prod_{h=0}^{H-1} \pi(a_{h+1}|a_h, s), \quad (7)$$

$$\pi_\theta(a_{0:H}|s) = \pi_\theta(a_H|s) \prod_{h=1}^H \pi_\theta(a_{h-1}|a_h, s). \quad (8)$$

The output $a = a_0$ constitutes the action, providing expressiveness for complex, multimodal distributions. This helps expose inherent computational bottlenecks in entropy estimation, motivating our proposed online MARL framework.

4 Bridge to OMAD and Theoretical Insight

Despite the generative prowess of diffusion models, their integration into online MARL is obstructed by three inherent mechanism mismatches as follows.

First, entropy-based exploration is hindered by intractable likelihoods. In contrast to the Gaussian policies, diffusion models lack tractable likelihoods [23]. This prohibits exact joint entropy compu-

tation, blocking maximum entropy objectives [41] crucial for preventing premature convergence in online MARL.

Second, an architectural conflict with CTDE complicates deployment. Standard monolithic backbones violate [76] the independence required for decentralized execution. Conversely, naive independent models fail to capture complex joint dependencies, necessitating a factorized design with decentralization to facilitate data collection.

Finally, a misalignment in coordination optimization persists as a significant open challenge. The policy’s iterative denoising nature inherently amplifies the difficulty of optimizing for sustained step-wise inter-agent coordination [45, 34]. Formulating a loss that effectively guides this multi-step generation towards global cooperation remains a significant algorithmic challenge.

To overcome these obstacles, we first establish a theoretical foundation for tractable entropy estimation. Assuming the joint policy factorizes as $\pi_{\theta}(a|s) = \prod_{i=1}^N \pi_{\theta_i}(a^i|s)$ [74], we leverage variational properties to derive a tractable lower bound, formalized as follows:

Theorem 1. (*Entropy Lower Bound for Decentralized Diffusion Policies*) *Given that the joint policy is factorized into independent diffusion processes, the entropy of the joint distribution $\mathcal{H}(\pi_{\theta}(a|s))$ is lower-bounded by the sum of individual variational bounds:*

$$\mathcal{H}(\pi_{\theta}(a|s)) \geq \sum_{i=1}^N l_{\pi_{\theta_i}}(a^i|s), \quad (9)$$

where $l_{\pi_{\theta_i}}(a^i|s) = \mathbb{E}_{\pi_{\theta_i}} \left[\log \frac{\pi_i(a_{1:H}^i|a_{0:H}^i,s)}{\pi_{\theta_i}(a_{0:H}^i|s)} \right]$ is the evidence lower bound for each agent.

Proof. (Sketch) The proof exploits the factorized structure of our multi-agent policy, which allows the intractable joint entropy to decompose into a summation of individual marginal entropies. We then derive a tractable evidence lower bound (ELBO) for each agent’s diffusion trajectory via variational inference to complete the proof. Detailed derivations are provided in Appendix B. \square

Since the exact computation of the joint policy entropy is intractable, the derived lower bound serves as a tractable surrogate for approximating the Maximum Entropy RL objective [20]. Facilitating this helps us effectively incentivize exploration while harnessing the high expressiveness of diffusion policies. This theoretical formulation lays the groundwork for our proposed OMAD algorithm, enabling efficient entropy-regularized MARL in an online setting under the CTDE framework.

5 The OMAD Method

This section introduces our proposed diffusion policy algorithm for online multi-agent reinforcement learning, with a systemic overview depicted in Figure 1. To tackle the challenges of applying diffusion models in online MARL, our framework integrates two strategic designs. (i) First, we

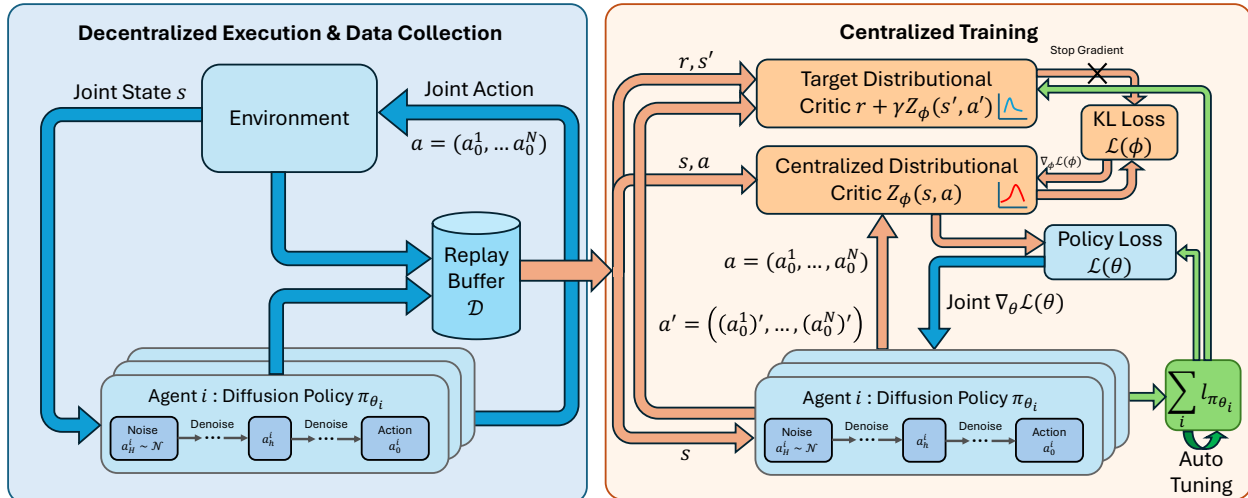


Figure 1: The CTDE framework of OMAD. The left panel illustrates Decentralized Execution, where agents independently sample actions via a denoising diffusion process. The right panel depicts Centralized Training, where a shared Distributional Critic provides unified Value Guidance to jointly optimize policies, stabilized by adaptive regularization for the entropy evidence lower bound.

construct a specialized network architecture that seamlessly unifies policy learning with iterative denoising action generation. (ii) Second, to strictly adhere to the CTDE paradigm, we introduce a centralized distributional critic. This critic plays a pivotal role in guiding synchronized policy training by maximizing a scaled joint entropy Evidence Lower Bound (ELBO). We detail the formulation and implementation of these components below.

5.1 Decentralized Diffusion Policy Formulation

To scale diffusion-based control to multi-agent domains, we employ a factorized policy architecture $\pi_{\theta}(a|s) = \prod_{i=1}^N \pi_{\theta_i}(a^i|s)$ [74]. This architecture, corresponding to the decentralized execution phase (blue region in Figure 1), eschews joint space modeling to ensure efficient data collection while retaining policy expressiveness.

We instantiate a reverse-time SDE introduced in Sec. 3.2 for each agent i , parameterizing the drift with a specific score network $f_{\theta_i}(a_t^i, s, t) \approx \nabla_{a_t^i} \log \pi_{i,t}(a_t^i|s)$. This decoupling facilitates efficient parallel sampling via the Euler-Maruyama solver, where the synchronized generation over H steps is governed by:

$$a_{h-1}^i = a_h^i + \underbrace{(\beta_h a_h^i + 2\eta^2 \beta_h f_{\theta_i}(a_h^i, s, t_h))}_{\text{Drift (Score Guidance)}} \delta + \xi_h^i, \quad (10)$$

where $t_h = hT/H$ and ξ_h^i follows Eq. (4). The action a_0^i is obtained by iteratively denoising $a_H^i \sim \mathcal{N}(0, \eta^2 I)$. Such scheme effectively captures complex multi-modal joint distributions through the composition of individual policies.

5.2 Online Centralized Training the Diffusion Policy

With the tractable entropy lower bound established in Theorem 1, we can now operationalize the Maximum Entropy principle within our multi-agent framework. Specifically, we substitute the computationally intractable exact entropy with the derived ELBO, utilizing it as a practical surrogate to guide exploration. This substitution enables stable and effective policy optimization even in high-dimensional joint action spaces. In this subsection, we formulate the overall objective for online centralized training, defining how the diffusion policy is jointly optimized with the scaled entropy regularization to balance reward maximization and exploration. This process corresponds to the orange-shaded phase on the right side of Figure 1.

Tractable Maximum Entropy MARL Objective. Leveraging the derived entropy evidence lower bound in Theorem 1, we formulate a tractable surrogate objective for Maximum Entropy MARL. In contrast to prior works that eschew entropy regularization [41] due to the intractable likelihoods of implicit policies, we explicitly incorporate the variational lower bound $l_{\pi_{\theta_i}}$ as an intrinsic exploration bonus. The resulting joint objective is to maximize the cumulative discounted sum of the reward and the scaled entropy surrogate:

$$J(\boldsymbol{\pi}_{\boldsymbol{\theta}}(\cdot|s)) := \mathbb{E}_{\boldsymbol{\pi}_{\boldsymbol{\theta}}} \left[\sum_{t=0}^{\infty} \sum_{i=1}^N \gamma^t (r_t^i + \alpha l_{\pi_{\theta_i}}(a_t^i, s_t)) \right]. \quad (11)$$

Here, $\alpha > 0$ is the temperature parameter regulating the stochasticity of the policy, consistent with the maximum entropy reinforcement learning framework [21]. This objective fundamentally transforms the optimization landscape: by maximizing Eq. (11), agents are driven to maximize expected returns while simultaneously maintaining high stochasticity in their diffusion policies, thereby preventing premature convergence.

To effectively optimize this tractable entropy-regularized objective, we adopt the CTDE paradigm. Crucially, we introduce a centralized distributional critic to model the value distribution of the joint state-action pairs, providing a more robust signal to guide the diffusion policy optimization.

Centralized Joint Distributional Critic Learning. To tackle the inherent multimodality of multi-agent diffusion, we propose a Joint Distributional Critic $Z_{\phi}(s, a)$. Departing from standard CTDE methods that compress returns into the expected joint return $Q_{\phi}(s, a) = \mathbb{E}[Z_{\phi}(s, a)]$, we model the full value distribution [4]. Crucially, this disentangles true coordination signals from the compounded stochasticity of interacting diffusion policies for robust supervision that stabilizes joint optimization.

We implement the critic (located in the top-right of Figure 1) using the CrossQ architecture [6] adapted for the multi-agent domain. We define the distributional Bellman operator applied to the joint return distribution. Specifically, the target distribution is constructed by augmenting shared rewards with the derived sum of individual entropy lower bounds, thereby enforcing a unified

objective:

$$\mathcal{T}Z_\phi(s, a) := \sum_{i=1}^N r^i + \gamma(Z_\phi(s', a') + \alpha \sum_{i=1}^N l_{\pi_{\theta_i}}((a')^i | s')), \quad (12)$$

where $a' = ((a')^1, \dots, (a')^N)$ denotes the joint action sampled from the target diffusion policies π_{θ_i} given the next state s' . Here, the equality holds in distribution. This formulation ensures that the critic evaluates the global quality of joint actions while accounting for the exploration bonuses of all agents, thereby aligning individual incentives with the global objective, which is written as:

$$\mathcal{L}(\phi) = \mathbb{E}[\text{KL}(Z_\phi(s, a), \text{sg}(\mathcal{T}Z_\phi(s, a)))] + \xi \mathcal{H}(Z_\phi(s, a)). \quad (13)$$

To efficiently optimize this target, we instantiate a multi-agent CrossQ [6] mechanism by combining stop-gradients $\text{sg}(\cdot)$ with input Batch Normalization, enabling high data efficiency without divergence. Furthermore, our entropy-regularized distributional critic (Z_ϕ with coefficient ξ) captures the granular uncertainty of joint interactions, surpassing expectation-based baselines.

Synchronized Diffusion Policy Optimization. We formulate the multi-agent policy optimization as an iterative projection problem, aiming to align the joint policy π_θ with the distribution derived by the learned critic, i.e., $\pi_\theta(a|s) \propto \exp(\frac{1}{\alpha} Q_\phi(s, a))$ corresponding to Eq. (2) (which is located in the bottom-right of Figure 1). This corresponds to minimizing the KL divergence term, expressed as: $D_{\text{KL}}(\pi_\theta(\cdot|s) \| \frac{1}{Z} \exp(\frac{1}{\alpha} Q_\phi(s, \cdot)))$. However, direct optimization is intractable due to the iterative diffusion process. We thus derive a tractable surrogate loss by expanding the divergence over latent trajectories, yielding a unified synchronized objective:

$$\mathcal{L}(\theta) = \mathbb{E} \left[\sum_{i=1}^N \log \pi_{\theta_i}(a_H^i | s) - \frac{1}{\alpha} Q_\phi(s, a_0) + \sum_{i=1}^N \sum_{h=1}^H \log \frac{\pi_{\theta_i}(a_{h-1}^i | a_h^i, s)}{\pi_i(a_h^i | a_{h-1}^i, s)} \right] + \log Z(s). \quad (14)$$

Here, a_0 denotes the terminal joint action synthesized through the synchronized reverse diffusion trajectories $\{a_H^i, \dots, a_0^i\}_{i=1}^N$ governed by Eq. (10), $\pi_i(a_h^i | a_{h-1}^i, s)$ represents the forward noising distribution constructed with $\frac{1}{Z(s)} \exp(\frac{1}{\alpha} Q_\phi(s, \cdot))$ as the target policy, and $Q_\phi(s, a_0) = \mathbb{E}[Z_\phi(s, a_0)]$ denotes the expectation of $Z_\phi(s, a_0)$. Crucially, this formulation establishes a shared optimization landscape where agents perform synchronized updates via a holistic loss. In stark contrast to decoupled approaches as HARL [74, 36] that rely on fragmented local losses, our method orchestrates a unified update guided by the global value function, ensuring superior coordination stability and efficiency. Detailed derivations of the objective function are provided in the Appendix C.

Variational Surrogate for Temperature Auto-Tuning. To dynamically regulate the exploration-exploitation trade-off without manual tuning, we formulate the temperature α adjustment as a dual constrained optimization problem (shaded green in Figure 1). Uniquely, we adapt the maximum entropy principle to the diffusion setting by enforcing a constraint on the *joint variational lower bound* rather than the intractable exact entropy. Specifically, we optimize α to maintain the aggregate

ELBO above a target threshold:

$$\mathcal{L}(\alpha) = \alpha \left(\mathcal{H}_{\text{target}} - \sum_{i=1}^N l_{\pi_{\theta_i}}(a^i | s) \right). \quad (15)$$

Here, $\mathcal{H}_{\text{target}}$ defines the minimum exploration budget. Minimizing this objective automatically scales α to maintain the aggregate ELBO at the target level.

OMAD establishes a tractable paradigm by deriving a decomposable entropy lower bound aligned with diffusion denoising. Our framework integrates a centralized distributional critic, synchronized policy updates, and auto-tuned temperature. This design ensures robust high-entropy coordination while preserving decentralized execution, providing a scalable foundation for diffusion-based online MARL.

5.3 Algorithm and Discussion

Algorithm 1 Online Multi-Agent Diffusion Policy (OMAD)

- 1: **Initialize:** Distributional state-action function $Z_\phi(s, a)$, diffusion policy and the target term $\pi_{\theta_i}, \pi_{\theta'_i}$ for $i = 1, 2, \dots, N$ agents, temperature α , policy delay d_l , target entropy $\mathcal{H}_{\text{target}}$, learning rate η , replay buffer \mathcal{D} and the threshold buffer size L_{init} . // Initialization
 - 2: **for** $m = 1$ to M episodes **do**
 - 3: Sample trajectory $(s_0, a_0, r_0, s_1, a_1, \dots, s_T, a_T, r_T)$ for T timesteps using $\pi_{\theta'_i}$ and insert them into \mathcal{D} . // Trajectory Generation
 - 4: **if** Buffer length $L_{\mathcal{D}} > L_{\text{init}}$ **then**
 - 5: Sample $B = \{(s, a, r, s')\}$ from \mathcal{D} . // Sampling
 - 6: Sample actions $a' = ((a')^1, \dots, (a')^N)$ using $\pi_{\theta'_i}$, calculate $\mathcal{L}(\phi)$ using Eq. (13) and optimize ϕ . // Critic Optimization
 - 7: **if** $m \bmod d_l = 0$ **then**
 - 8: Sample actions $a = (a^1, \dots, a^N)$ using π_{θ_i} , calculate $\mathcal{L}(\theta)$ using Eq. (14) and jointly optimize $\{\theta_i\}_{i=1}^N$. // Diffusion Policy Optimization
 - 9: **end if**
 - 10: Calculate $l_{\pi_{\theta_i}}$ and optimize the temperature α via minimizing Eq. (15). // Temperature Optimization
 - 11: Update target networks $\theta'_i \leftarrow \rho \theta'_i + (1 - \rho) \theta_i$. // Target Network Optimization
 - 12: **end if**
 - 13: **end for**
-

The training procedure of the proposed online multi-agent diffusion policy is summarized in Algorithm 1. Line 1 initializes the distributional critic, diffusion policies for all agents, target networks, and the replay buffer. Line 3 collects trajectories by executing the target diffusion policies and stores the resulting transitions for off-policy learning. When the replay buffer is sufficiently populated, Line 5 samples mini-batches for training. Line 6 updates the distributional state-action value function using actions sampled from the target diffusion policies. Line 8 jointly optimizes the diffusion policies by minimizing the diffusion-based policy objective guided by the learned distributional critic. Line 9 adapts the entropy temperature to enforce the target entropy, and Line 10

softly updates the target policy networks to stabilize training.

OMAD pioneers online diffusion-based MARL, departing from restrictive Gaussian policies used in methods, including HARL [74, 36]. By modeling policies as generative diffusion processes, OMAD captures complex, multi-modal joint action distributions essential for sophisticated coordination. Distinct from discrete-time [61, 41] or deterministic ODE-based approaches [16], OMAD employs an SDE formulation to ensure sustained stochasticity. Advancing beyond DIME [8], we derive a factorized entropy bound with a centralized distributional critic to address non-stationarity, offering a sample-efficient off-policy alternative to HADQ [3].

Overall, OMAD synergizes a centralized distributional critic with synchronized diffusion policies within a tractable variational framework, establishing a robust off-policy paradigm ensuring scalable, sample-efficient coordination. We next empirically validate how OMAD’s high expressiveness manifests as efficient exploration and superior performance.

6 Experiments

We empirically validate the efficacy of OMAD across diverse continuous-control multi-agent benchmarks. In this section, we detail our experimental setup and present a rigorous comparative analysis against state-of-the-art baselines. Notably, we visually demonstrate how diffusion expressiveness unlocks superior state exploration. Finally, we conduct ablation studies to isolate the contribution of each key algorithmic component, empirically justifying the rationality of our proposed framework.

6.1 Experiment Setup

Environments. We evaluate our method on two widely adopted multi-agent benchmarks: the Multi-Agent Particle Environments (MPE) [37] and the challenging, high-dimensional Multi-Agent MuJoCo (MAMuJoCo) tasks [47]. We evaluate on representative tasks from MPE (Physical Deception, Cooperative Navigation) involving particle cooperation, and MAMuJoCo (HalfCheetah, Ant, Walker, Swimmer) requiring coordinated locomotion. Details are provided in Appendix D.1.

Baselines: We compare our algorithm with the following state-of-the-art baseline online MARL algorithms: HATD3 [74] and HASAC [36]. Besides, we compare our algorithm with the extension of the single-agent diffusion-based policy as MADPMD and MASDAC [41]. Each algorithm is executed for 5 random seeds and the mean performance and the standard deviation for 10 episodes are presented. A detailed description of hyperparameters, neural network structures, and setup can be found in Appendix D.2.

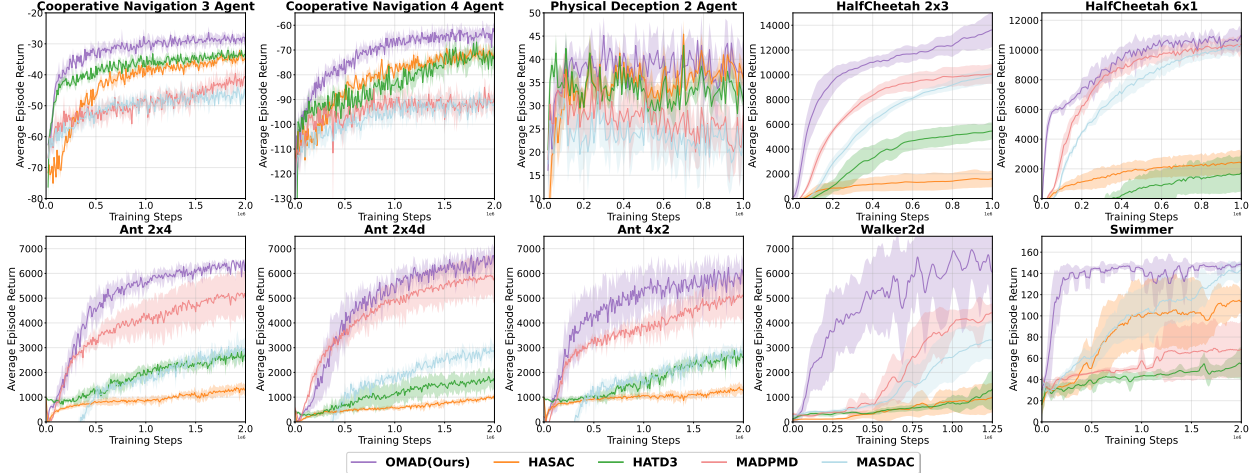


Figure 2: Learning curves comparing OMAD with state-of-the-art online MARL baselines (HATD3 and HASAC) and two representative extensions of the diffusion policies (MADPMD and MASDAC) on MPE and MAMuJoCo benchmarks. The plots report the average episode return over training steps, averaged across 5 random seeds, with shaded regions indicating one standard deviation. Results demonstrate that OMAD consistently achieves faster convergence and superior final performance across both low-dimensional MPE tasks and high-dimensional continuous control environments.

6.2 Experiment Results

The experimental results in different tasks are shown in Figure 2. Our method consistently outperforms all compared baselines across a wide range of cooperative and competitive tasks, including MPE and challenging MAMuJoCo benchmarks. In low-dimensional MPE tasks, OMAD achieves faster convergence and higher final returns, reducing training steps to reach baseline peaks by up to $5\times$. This indicates improved coordination efficiency and training stability compared to both value-based and diffusion-based baselines. Notably, while MADPMD and MASDAC benefit from diffusion modeling, they exhibit slower convergence or inferior asymptotic performance, suggesting that directly extending diffusion policies to multi-agent settings is insufficient without effective centralized training and value guidance.

In high-dimensional continuous control environments such as Ant (2×4 , $2\times 4d$, 4×2), HalfCheetah (2×3 , 6×1), Walker2d (2×3), and Swimmer (2×1), OMAD demonstrates substantial performance gains with lower variance and exhibits a consistent $2.5\sim 5\times$ speedup in sample efficiency compared to the strongest baselines across these complex dynamics. These results highlight the scalability of our approach and its robustness in complex dynamics with strong inter-agent coupling. Overall, the empirical results validate that integrating diffusion-based policy generation with centralized value modeling leads to more stable learning and superior performance in both low- and high-dimensional multi-agent environments.

To empirically validate the exploration benefits conferred by the high expressiveness of our diffusion

policies, we analyze the state distributions accumulated in the replay buffers after the first 250k training steps under the *Ant* 2×4 task. We discretize the 2D state space (dimensions 1 and 21 corresponding to the agent’s spatial navigation) over the range $[-19, 18] \times [-16, 19]$ with a grid interval of 0.5, resulting in a total of 1368 bins. Under this metric, OMAD achieves the broadest coverage of 68.3% (both blue and orange areas), representing a significant relative improvement of 41% and 24% over HATD3 (48.4%) and HASAC (55.0%), respectively. The regions highlighted in orange represent state spaces uniquely explored by OMAD, providing compelling evidence that the superior expressiveness of our entropy-regularized diffusion policy empowers the agent to escape local optima and cover a substantially wider solution space.

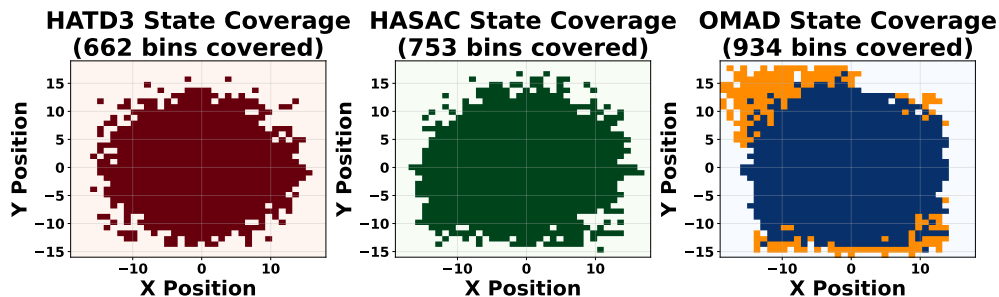


Figure 3: State coverage comparison on representative dimensions (1 and 21) at 250k steps. We visualize the state occupancy within the replay buffers for HATD3, HASAC, and OMAD. Colored regions (red, green, blue and orange) indicate visited states. OMAD achieves the broadest coverage, where orange regions are uniquely explored by OMAD, demonstrating superior exploration.

6.3 Ablation Study

To investigate the sensitivity of OMAD, we perform a detailed ablation studies on the *Ant* 2×4 task (10^6 steps) to isolate the impact of three key components: (1) distributional hyperparameters (V_{\max} and atom count); (2) diffusion denoising steps; and (3) the scaled entropy coefficient α .

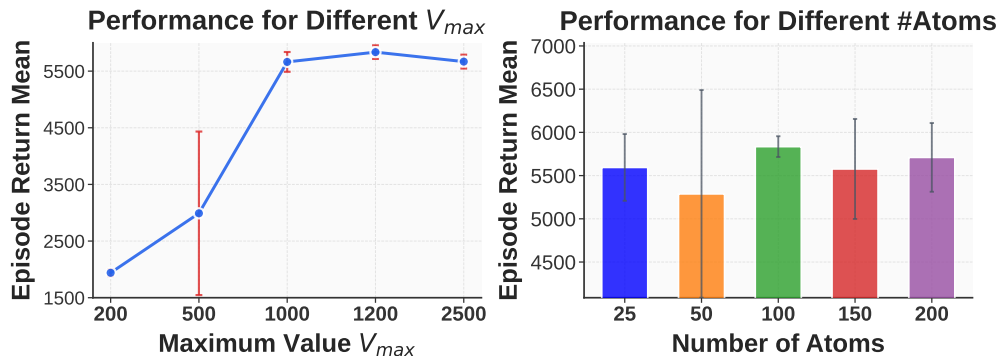


Figure 4: Ablation study on Distributional Q-function hyperparameters. **Left:** The sensitivity of the agent’s performance to the support upper bound V_{\max} . **Right:** The impact of the discretization resolution on performance for different number of atoms.

Impact of Distributional Hyperparameters. Figure 4 (Left) highlights the sensitivity to

the value support V_{\max} . Low thresholds (e.g., 200) severely hamper performance via truncation, whereas performance stabilizes around $V_{\max} = 1000$, effectively covering expected returns. Regarding granularity (Figure 4, Right), while generally robust, we identify 100 intervals (101 atoms). Lower resolutions fail to capture distribution complexity, while higher ones yield diminishing returns. We thus adopt $V_{\max} = 1200$ and 100 intervals.

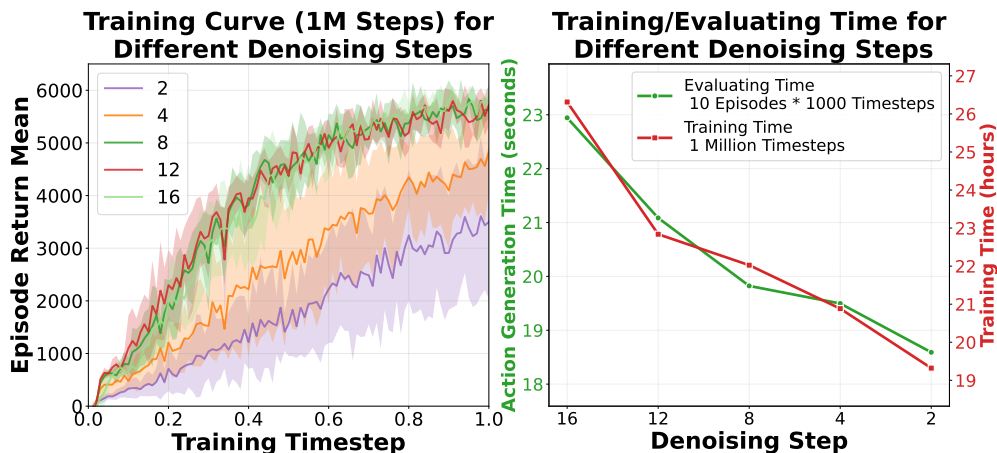


Figure 5: Ablation study on the number of denoising steps. **Left:** Episode return curves during training for varying denoising steps. **Right:** The trade-off between computational cost (training/inference time) and the number of steps.

Impact of Denoising Steps. We analyze the performance-efficiency trade-off by varying denoising steps (Figure 5). Performance saturates at 8 steps (≈ 6000 return), matching 12 and 16-step models, whereas 2 and 4-step variants underperform (< 4500). Conversely, computational costs increase linearly: raising steps from 8 to 16 increases training time from 22h to 26h and latency by $\sim 3s$. Consequently, we select 8 steps as the optimal balance, achieving asymptotic performance with minimal overhead.

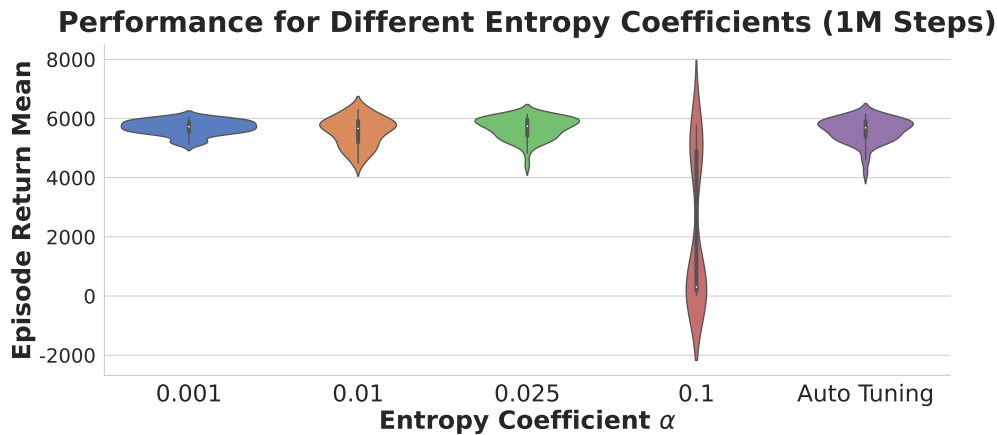


Figure 6: Efficacy of Auto-Tuning vs. Fixed Entropy Coefficients.

Impact of Adaptive Entropy Regularization. As illustrated in Figure 6, training OMAD algo-

rithm exhibits high sensitivity to the entropy coefficient α . A large fixed coefficient ($\alpha = 0.1$) injects excessive stochasticity, destabilizing the denoising process and preventing convergence. Conversely, while manually tuned smaller values ($\alpha \in \{0.001, 0.01\}$) yield high returns, they lack adaptability. Crucially, our Auto-Tuning mechanism outperforms this rigid paradigm. By dynamically modulating α , it flexibly balances exploration and exploitation, matching the peak performance (≈ 6000) of the best fixed settings. This adaptive capability eliminates the need for exhaustive hyperparameter search, facilitating the efficient and robust training of expressive diffusion policies.

7 Conclusion

We present OMAD, a pioneering framework that unlocks online diffusion-based MARL via a tractable variational lower bound for joint entropy. By synergizing this principled exploration with a centralized distributional critic, OMAD robustly mitigates non-stationarity and ensures stable coordination. Empirical results across MPE and MAMuJoCo confirm that OMAD establishes a new state-of-the-art, significantly outperforming both strong value-based baselines and naive diffusion extensions in sample efficiency and asymptotic performance.

Impact Statement

This paper presents work whose goal is to advance the field of Machine Learning. There are many potential societal consequences of our work, none which we feel must be specifically highlighted here.

References

- [1] Johannes Ackermann, Volker Gabler, Takayuki Osa, and Masashi Sugiyama. Reducing over-estimation bias in multi-agent domains using double centralized critics. *Advances in Neural Information Processing Systems: Deep Reinforcement Learning Workshop*, 2019.
- [2] Anurag Ajay, Yilun Du, Abhi Gupta, Joshua B Tenenbaum, Tommi S Jaakkola, and Pulkit Agrawal. Is conditional generative modeling all you need for decision making? In *The Eleventh International Conference on Learning Representations*, 2023.
- [3] Anonymous. Heterogeneous agent q-weighted policy optimization. In *Submitted to The Fourteenth International Conference on Learning Representations*, 2025. under review.
- [4] Marc G Bellemare, Will Dabney, and Rémi Munos. A distributional perspective on reinforcement learning. In *International conference on machine learning*, pages 449–458. PMLR, 2017.
- [5] Daniel S Bernstein, Robert Givan, Neil Immerman, and Shlomo Zilberstein. The complexity of decentralized control of markov decision processes. *Mathematics of operations research*, 27(4):819–840, 2002.

- [6] Aditya Bhatt, Daniel Palenicek, Boris Belousov, Max Argus, Artemij Amiranashvili, Thomas Brox, and Jan Peters. Crossq: Batch normalization in deep reinforcement learning for greater sample efficiency and simplicity. In *The Twelfth International Conference on Learning Representations*, 2024.
- [7] Tim Brooks, Bill Peebles, Connor Holmes, Will DePue, Yufei Guo, Li Jing, David Schnurr, Joe Taylor, Troy Luhman, Eric Luhman, Clarence Ng, Ricky Wang, and Aditya Ramesh. Video generation models as world simulators. *OpenAI Blog*, 2024.
- [8] Onur Celik, Zechu Li, Denis Blessing, Ge Li, Daniel Palenicek, Jan Peters, Georgia Chalvatzaki, and Gerhard Neumann. Dime: Diffusion-based maximum entropy reinforcement learning. In *Forty-second International Conference on Machine Learning*, 2025.
- [9] Huayu Chen, Cheng Lu, Chengyang Ying, Hang Su, and Jun Zhu. Offline reinforcement learning via high-fidelity generative behavior modeling. In *The Eleventh International Conference on Learning Representations*, 2023.
- [10] Junhong Chen, Ziqi Yang, Haoyuan G Xu, Dandan Zhang, and George Mylonas. Multi-agent systems for robotic autonomy with llms. In *Proceedings of the Computer Vision and Pattern Recognition Conference*, pages 4194–4204, 2025.
- [11] Yangkun Chen, Kai Yang, Jian Tao, and Jiafei Lyu. Novelty-guided data reuse for efficient and diversified multi-agent reinforcement learning. In *Proceedings of the AAAI Conference on Artificial Intelligence*, volume 39, pages 15930–15938, 2025.
- [12] HUA Chengxiu, Jiawen Gu, and Yushun Tang. Continuous q-score matching: Diffusion guided reinforcement learning for continuous-time control. In *The Thirty-ninth Annual Conference on Neural Information Processing Systems*, 2025.
- [13] Cheng Chi, Siyuan Feng, Yilun Du, Zhenjia Xu, Eric Cousineau, Benjamin Burchfiel, and Shuran Song. Diffusion policy: Visuomotor policy learning via action diffusion. In *Proceedings of Robotics: Science and Systems (RSS)*, 2023.
- [14] Christian Schroeder de Witt, Tarun Gupta, Denys Makoviichuk, Viktor Makoviychuk, Philip HS Torr, Mingfei Sun, and Shimon Whiteson. Is independent learning all you need in the starcraft multi-agent challenge? *arXiv preprint arXiv:2011.09533*, 2020.
- [15] Shutong Ding, Ke Hu, Zhenhao Zhang, Kan Ren, Weinan Zhang, Jingyi Yu, Jingya Wang, and Ye Shi. Diffusion-based reinforcement learning via q-weighted variational policy optimization. In *The Thirty-eighth Annual Conference on Neural Information Processing Systems*, 2024.
- [16] Xiaoyi Dong, Jian Cheng, and Xi Sheryl Zhang. Maximum entropy reinforcement learning with diffusion policy. In *Forty-second International Conference on Machine Learning*, 2025.

- [17] Linjiajie Fang, Ruoxue Liu, Jing Zhang, Wenjia Wang, and Bingyi Jing. Diffusion actor-critic: Formulating constrained policy iteration as diffusion noise regression for offline reinforcement learning. In *The Thirteenth International Conference on Learning Representations*, 2024.
- [18] Jakob Foerster, Gregory Farquhar, Triantafyllos Afouras, Nantas Nardelli, and Shimon Whiteson. Counterfactual multi-agent policy gradients. In *Proceedings of the AAAI conference on artificial intelligence*, volume 32, 2018.
- [19] Yuqian Fu, Yuanheng Zhu, Jian Zhao, Jiajun Chai, and Dongbin Zhao. INS: Interaction-aware synthesis to enhance offline multi-agent reinforcement learning. In *The Thirteenth International Conference on Learning Representations*, 2025.
- [20] Tuomas Haarnoja, Haoran Tang, Pieter Abbeel, and Sergey Levine. Reinforcement learning with deep energy-based policies. In *International conference on machine learning*, pages 1352–1361. PMLR, 2017.
- [21] Tuomas Haarnoja, Aurick Zhou, Pieter Abbeel, and Sergey Levine. Soft actor-critic: Off-policy maximum entropy deep reinforcement learning with a stochastic actor. In *International conference on machine learning*, pages 1861–1870. Pmlr, 2018.
- [22] Philippe Hansen-Estruch, Ilya Kostrikov, Michael Janner, Jakub Grudzien Kuba, and Sergey Levine. Idql: Implicit q-learning as an actor-critic method with diffusion policies. *arXiv preprint arXiv:2304.10573*, 2023.
- [23] Jonathan Ho, Ajay Jain, and Pieter Abbeel. Denoising diffusion probabilistic models. *Advances in Neural Information Processing Systems*, 33:6840–6851, 2020.
- [24] Xiaoliang Hu, Fuyun Wang, Tong Zhang, and Zhen Cui. Value diffusion reinforcement learning. In *The Thirty-ninth Annual Conference on Neural Information Processing Systems*, 2025.
- [25] Xiaoyu Huang, Yufeng Chi, Ruofeng Wang, Zhongyu Li, Xue Bin Peng, Sophia Shao, Borivoje Nikolic, and Koushil Sreenath. Diffuseloco: Real-time legged locomotion control with diffusion from offline datasets. In *8th Annual Conference on Robot Learning*, 2024.
- [26] Xiaoyu Huang, Yufeng Chi, Ruofeng Wang, Zhongyu Li, Xue Bin Peng, Sophia Shao, Borivoje Nikolic, and Koushil Sreenath. Diffuseloco: Real-time legged locomotion control with diffusion from offline datasets. In *Conference on Robot Learning*, pages 1567–1589. PMLR, 2025.
- [27] Michael Janner, Yilun Du, Joshua Tenenbaum, and Sergey Levine. Planning with diffusion for flexible behavior synthesis. In *International Conference on Machine Learning*, 2022.
- [28] Whiyoung Jung, Sunghoon Hong, Deunsol Yoon, Kanghoon Lee, and Woohyung Lim. Agent-centric actor-critic for asynchronous multi-agent reinforcement learning. In *Forty-second International Conference on Machine Learning*, 2025.

- [29] Bingyi Kang, Xiao Ma, Chao Du, Tianyu Pang, and Shuicheng Yan. Efficient diffusion policies for offline reinforcement learning. *Advances in Neural Information Processing Systems*, 36:67195–67212, 2023.
- [30] Andreas Kontogiannis, Konstantinos Papathanasiou, Yi Shen, Giorgos Stamou, Michael M Zavlanos, and George Vouros. Enhancing cooperative multi-agent reinforcement learning with state modelling and adversarial exploration. In *Forty-second International Conference on Machine Learning*, 2025.
- [31] Jaewoo Lee, Sujin Yun, Taeyoung Yun, and Jinkyoo Park. Gta: Generative trajectory augmentation with guidance for offline reinforcement learning. *Advances in Neural Information Processing Systems*, 37:56766–56801, 2024.
- [32] Chao Li, Ziwei Deng, Chenxing Lin, Wenqi Chen, Yongquan Fu, Weiquan Liu, Chenglu Wen, Cheng Wang, and Siqi Shen. Dof: A diffusion factorization framework for offline multi-agent decision making. In *International Conference on Learning Representations*, 2025.
- [33] Pengyi Li, Jianye Hao, Hongyao Tang, Yan Zheng, and Xian Fu. Race: improve multi-agent reinforcement learning with representation asymmetry and collaborative evolution. In *International Conference on Machine Learning*, pages 19490–19503. PMLR, 2023.
- [34] Yueheng Li, Guangming Xie, and Zongqing Lu. Revisiting cooperative off-policy multi-agent reinforcement learning. In *Forty-second International Conference on Machine Learning*, 2025.
- [35] Zhuoran Li, Ling Pan, and Longbo Huang. Beyond conservatism: Diffusion policies in offline multi-agent reinforcement learning, 2023.
- [36] Jiarong Liu, Yifan Zhong, Siyi Hu, Haobo Fu, QIANG FU, Xiaojun Chang, and Yaodong Yang. Maximum entropy heterogeneous-agent reinforcement learning. In *The Twelfth International Conference on Learning Representations*, 2024.
- [37] Ryan Lowe, Yi I Wu, Aviv Tamar, Jean Harb, OpenAI Pieter Abbeel, and Igor Mordatch. Multi-agent actor-critic for mixed cooperative-competitive environments. *Advances in neural information processing systems*, 30, 2017.
- [38] Cheng Lu, Huayu Chen, Jianfei Chen, Hang Su, Chongxuan Li, and Jun Zhu. Contrastive energy prediction for exact energy-guided diffusion sampling in offline reinforcement learning. In *International Conference on Machine Learning*, pages 22825–22855. PMLR, 2023.
- [39] Cheng Lu, Yuhao Zhou, Fan Bao, Jianfei Chen, Chongxuan Li, and Jun Zhu. Dpm-solver: A fast ode solver for diffusion probabilistic model sampling in around 10 steps. *Advances in neural information processing systems*, 35:5775–5787, 2022.
- [40] Cong Lu, Philip Ball, Yee Whye Teh, and Jack Parker-Holder. Synthetic experience replay. *Advances in Neural Information Processing Systems*, 36:46323–46344, 2023.

- [41] Haitong Ma, Tianyi Chen, Kai Wang, Na Li, and Bo Dai. Efficient online reinforcement learning for diffusion policy. In *Forty-second International Conference on Machine Learning*, 2025.
- [42] Laëtitia Matignon, Laurent Jeanpierre, and Abdel-illah Mouaddib. Coordinated multi-robot exploration under communication constraints using decentralized markov decision processes. In *Twenty-sixth AAAI conference on artificial intelligence*, 2012.
- [43] Frans A Oliehoek and Christopher Amato. *A concise introduction to decentralized POMDPs*. Springer, 2016.
- [44] Frans A Oliehoek, Matthijs TJ Spaan, and Nikos Vlassis. Optimal and approximate q-value functions for decentralized pomdps. *Journal of Artificial Intelligence Research*, 32:289–353, 2008.
- [45] Ling Pan, Tabish Rashid, Bei Peng, Longbo Huang, and Shimon Whiteson. Regularized softmax deep multi-agent q-learning. *Advances in Neural Information Processing Systems*, 34:1365–1377, 2021.
- [46] Tim Pearce, Tabish Rashid, Anssi Kanervisto, Dave Bignell, Mingfei Sun, Raluca Georgescu, Sergio Valcarcel Macua, Shan Zheng Tan, Ida Momennejad, Katja Hofmann, et al. Imitating human behaviour with diffusion models. In *The Eleventh International Conference on Learning Representations*, 2024.
- [47] Bei Peng, Tabish Rashid, Christian Schroeder de Witt, Pierre-Alexandre Kamienny, Philip Torr, Wendelin Böhmer, and Shimon Whiteson. Facmac: Factored multi-agent centralised policy gradients. *Advances in Neural Information Processing Systems*, 34:12208–12221, 2021.
- [48] Michael Psenka, Alejandro Escontrela, Pieter Abbeel, and Yi Ma. Learning a diffusion model policy from rewards via q-score matching. In *International Conference on Machine Learning*, pages 41163–41182. PMLR, 2024.
- [49] Dan Qiao, Wenhao Li, Shanchao Yang, Hongyuan Zha, and Baoxiang Wang. Offline multi-agent reinforcement learning via score decomposition, 2025.
- [50] Tabish Rashid, Mikayel Samvelyan, Christian Schroeder, Gregory Farquhar, Jakob Foerster, and Shimon Whiteson. Qmix: Monotonic value function factorisation for deep multi-agent reinforcement learning. In *International conference on machine learning*, pages 4295–4304. PMLR, 2018.
- [51] Allen Z Ren, Justin Lidard, Lars Lien Ankile, Anthony Simeonov, Pulkit Agrawal, Anirudha Majumdar, Benjamin Burchfiel, Hongkai Dai, and Max Simchowitz. Diffusion policy policy optimization. In *CoRL 2024 Workshop on Mastering Robot Manipulation in a World of Abundant Data*, 2024.
- [52] Simo Särkkä and Arno Solin. *Applied stochastic differential equations*, volume 10. Cambridge University Press, 2019.

- [53] Jascha Sohl-Dickstein, Eric Weiss, Niru Maheswaranathan, and Surya Ganguli. Deep unsupervised learning using nonequilibrium thermodynamics. In *International Conference on Machine Learning*, pages 2256–2265. PMLR, 2015.
- [54] Kyunghwan Son, Daewoo Kim, Wan Ju Kang, David Earl Hostallero, and Yung Yi. Qtran: Learning to factorize with transformation for cooperative multi-agent reinforcement learning. In *International conference on machine learning*, pages 5887–5896. PMLR, 2019.
- [55] Yang Song and Stefano Ermon. Generative modeling by estimating gradients of the data distribution. *Advances in Neural Information Processing Systems*, 32, 2019.
- [56] Yang Song, Jascha Sohl-Dickstein, Diederik P Kingma, Abhishek Kumar, Stefano Ermon, and Ben Poole. Score-based generative modeling through stochastic differential equations. In *International Conference on Learning Representations*, 2021.
- [57] Peter Sunehag, Guy Lever, Audrunas Gruslys, Wojciech Marian Czarnecki, Vinicius Zambaldi, Max Jaderberg, Marc Lanctot, Nicolas Sonnerat, Joel Z Leibo, Karl Tuyls, et al. Value-decomposition networks for cooperative multi-agent learning based on team reward. In *Proceedings of the 17th International Conference on Autonomous Agents and MultiAgent Systems*, pages 2085–2087, 2018.
- [58] Ardi Tampuu, Tambet Matiisen, Dorian Kodelja, Ilya Kuzovkin, Kristjan Korjus, Juhan Aru, Jaan Aru, and Raul Vicente. Multiagent cooperation and competition with deep reinforcement learning. *PloS one*, 12(4):e0172395, 2017.
- [59] Ming Tan. Multi-agent reinforcement learning: Independent vs. cooperative agents. In *Proceedings of the tenth international conference on machine learning*, pages 330–337, 1993.
- [60] Jianhao Wang, Zhizhou Ren, Terry Liu, Yang Yu, and Chongjie Zhang. Qplex: Duplex dueling multi-agent q-learning. In *International Conference on Learning Representations*, 2021.
- [61] Yinuo Wang, Likun Wang, Yuxuan Jiang, Wenjun Zou, Tong Liu, Xujie Song, Wenxuan Wang, Liming Xiao, Jiang Wu, Jingliang Duan, et al. Diffusion actor-critic with entropy regulator. In *Advances in Neural Information Processing Systems*, 2024.
- [62] Yinuo Wang, Likun Wang, Mining Tan, Wenjun Zou, Xujie Song, Wenxuan Wang, Tong Liu, Guojian Zhan, Tianze Zhu, Shiqi Liu, et al. Enhanced dacer algorithm with high diffusion efficiency. *arXiv preprint arXiv:2505.23426*, 2025.
- [63] Zhendong Wang, Jonathan J Hunt, and Mingyuan Zhou. Diffusion policies as an expressive policy class for offline reinforcement learning. In *The Eleventh International Conference on Learning Representations*, 2023.
- [64] Ziqi Wang, Jiashun Liu, and Ling Pan. Learning intractable multimodal policies with reparameterization and diversity regularization. In *The Thirty-ninth Annual Conference on Neural Information Processing Systems*, 2025.

- [65] Amber Xie, Oleh Rybkin, Dorsa Sadigh, and Chelsea Finn. Latent diffusion planning for imitation learning. In *Forty-second International Conference on Machine Learning*, 2025.
- [66] Guang Yang, Jingwen Qiao, Tianpei Yang, Yanqing Wu, Jing Huo, Xingguo Chen, and Yang Gao. Multi-agent reinforcement learning with communication-constrained priors. In *The Thirty-ninth Annual Conference on Neural Information Processing Systems*, 2025.
- [67] Long Yang, Zhixiong Huang, Fenghao Lei, Yucun Zhong, Yiming Yang, Cong Fang, Shiting Wen, Binbin Zhou, and Zhouchen Lin. Policy representation via diffusion probability model for reinforcement learning. *arXiv preprint arXiv:2305.13122*, 2023.
- [68] Ningyuan Yang, Jiaxuan Gao, Feng Gao, Yi Wu, and Chao Yu. Fine-tuning diffusion policies with backpropagation through diffusion timesteps, 2025.
- [69] Chao Yu, Akash Velu, Eugene Vinitzky, Jiaxuan Gao, Yu Wang, Alexandre Bayen, and Yi Wu. The surprising effectiveness of ppo in cooperative multi-agent games. *Advances in neural information processing systems*, 35:24611–24624, 2022.
- [70] Jintao Zhang, Kaiwen Zheng, Kai Jiang, Haoxu Wang, Ion Stoica, Joseph E Gonzalez, Jianfei Chen, and Jun Zhu. Turbodiffusion: Accelerating video diffusion models by 100-200 times. *arXiv preprint arXiv:2512.16093*, 2025.
- [71] Lvmin Zhang, Anyi Rao, and Maneesh Agrawala. Adding conditional control to text-to-image diffusion models. In *Proceedings of the IEEE/CVF international conference on computer vision*, pages 3836–3847, 2023.
- [72] Lvmin Zhang, Anyi Rao, and Maneesh Agrawala. Scaling in-the-wild training for diffusion-based illumination harmonization and editing by imposing consistent light transport. In *The Thirteenth International Conference on Learning Representations*, 2025.
- [73] Yang Zhang, Xinran Li, Jianing Ye, Shuang Qiu, Delin Qu, Xiu Li, Chongjie Zhang, and Chenjia Bai. Revisiting multi-agent world modeling from a diffusion-inspired perspective. In *The Thirty-ninth Annual Conference on Neural Information Processing Systems*, 2025.
- [74] Yifan Zhong, Jakub Grudzien Kuba, Xidong Feng, Siyi Hu, Jiaming Ji, and Yaodong Yang. Heterogeneous-agent reinforcement learning. *Journal of Machine Learning Research*, 25(32):1–67, 2024.
- [75] Ming Zhou, Jun Luo, Julian Villella, Yaodong Yang, David Rusu, Jiayu Miao, Weinan Zhang, Montgomery Alban, Iman Fadakar, Zheng Chen, et al. Smarts: An open-source scalable multi-agent rl training school for autonomous driving. In *Conference on robot learning*, pages 264–285. PMLR, 2021.
- [76] Zhengbang Zhu, Minghuan Liu, Liyuan Mao, Bingyi Kang, Minkai Xu, Yong Yu, Stefano Ermon, and Weinan Zhang. Madiff: Offline multi-agent learning with diffusion models. *Advances in Neural Information Processing Systems*, 37:4177–4206, 2024.

[77] Brian D Ziebart, Andrew L Maas, J Andrew Bagnell, Anind K Dey, et al. Maximum entropy inverse reinforcement learning. In *Aaai*, volume 8, pages 1433–1438. Chicago, IL, USA, 2008.

A Detailed Related Works

Here we propose our detailed related works about online MARL, diffusion policies in offline RL and single-agent online RL scenarios. We also discuss online MARL challenges and compare OMAD against baselines.

A.1 Online MARL

Online multi-agent reinforcement learning (MARL) has achieved substantial progress in recent years. Under the centralized training with decentralized execution (CTDE) paradigm [44, 42], a series of influential algorithms, including MADDPG [37], MAPPO [69], VDN [57], COMA [18], QTRAN [54] QMIX [50], and QPLEX [60] have significantly improved coordination and stability in cooperative tasks. In parallel, fully decentralized approaches such as IQL [58], IPPO [14], and MATD3 [1] achieve competitive performance without centralized critics, underscoring the scalability of online MARL.

Recent advances further enhance robustness, exploration efficiency, and scalability, including RES-QMIX [45], RACE [33], RCO [34], ACAC [28], MANGER [11], and SMPE [30], as well as studies on communication-constrained MARL [66]. More recently, heterogeneity-aware frameworks such as HARL and its variants (HATRPO, HAPPO, HATD3, HASAC) [74, 36], provide principled solutions for coordinating heterogeneous agents and mitigating non-stationarity, representing the state of the art in online MARL.

A.2 Diffusion Policy in Offline RL

Diffusion-based generative models have achieved remarkable success in representing complex probability distributions with superior expressiveness and multimodality, demonstrating outstanding performance in image and video generation [53, 55, 23, 56, 39, 71, 7, 72, 70]. These advantages naturally benefit sequential decision-making problems, leading to the introduction of diffusion policies in imitation learning [46, 65], where expert datasets are available. In offline RL [63], diffusion models have been explored for trajectory generation, e.g., Diffuser [27] and Decision Diffuser [2], expressive policy representations including Diff-QL [63], SfBC [9], EDP [29], IDQL [22], CEP [38], DAC [17], value representations (VDQL [24]), data augmentation, for instance, SynthER [40] and GTA [31] and robot learning [13, 26].

Recent offline MARL methods leverage diffusion models for multi-modality and data scarcity, including trajectory modeling (MADiff [76], DoF [32]), data synthesis (INS [19]), diverse action generation (DOM2 [35]), and score decomposition (OMSD [49]). However, relying strictly on fixed,

pre-collected datasets, offline MARL creates a fundamental gap from online settings, as it circumvents the critical need for active, coordinated exploration in non-stationary environments essential to tackle the severe non-stationary environments.

A.3 Diffusion Policy in Online RL

In online RL, the optimal policy cannot be directly sampled and must be learned via return- or value-based optimization, posing a fundamental challenge. To address this challenge, recent online diffusion-based RL methods adopt value-guided training, including gradient-updated behavior cloning (DIPO [67], DPPO [51] and DRAC [64]), Q-gradient score matching (QSM [48], CQSM [12]), entropy-controlled backpropagation through diffusion chains (DACER [61], DACER-v2 [62], DIME [8] and NCDPO [68]), score approximation (MaxEntDP [16]) and Q-weighted diffusion objectives with uniform exploration (QVPO [15], HAQO [3] and RSM [41]). In spite of policy-centric approaches, DIMA [73] uses diffusion models as environment dynamics to boost data efficiency.

However, extending these methods to online MARL faces three hurdles: computational inefficiency, as gradient propagation through diffusion chains [61] scales poorly with the number of agents; ineffective exploration, where simple heuristics [16] fail in high-dimensional joint spaces; and lack of coordination, as single-agent designs ignore non-stationarity inherent in multi-agent systems. To the best of our knowledge, our work is among the first to propose an efficient, off-policy diffusion framework specifically designed to overcome these hurdles, achieving superior training efficiency and coordination in online MARL.

To the best of our knowledge, OMAD pioneers the integration of diffusion-based policies into the realm of online multi-agent reinforcement learning. This represents a fundamental paradigm shift from existing architectures such as HARL [74, 36]. While these conventional methods rely on restrictive parametric representations (e.g., Gaussian policies) that limit agents to uni-modal behaviors, OMAD explicitly models the policy as a generative diffusion process. This innovation unlocks the capacity to capture highly complex, multi-modal joint action distributions essential for sophisticated coordination.

Compared to single-agent diffusion baselines, OMAD represents a significant leap in maximizing entropy for continuous-time denoising diffusion policies. While prior works such as DACER [61], DPMD and SDAC [41] rely on discrete-time formulations, and MaxEntRL [16] employs deterministic ODE sampling, OMAD leverages an efficient SDE-based formulation to ensure sustained stochasticity. Advancing beyond DIME [8], we derive a factorized joint entropy bound augmented by a centralized distributional critic to tackle non-stationarity. This yields a robust off-policy framework that, in spite of the on-policy HADQ [3], significantly enhances sample efficiency and data reuse.

B Proof of Theorem 1

Proof: Notice that the definition of the entropy about the joint action distribution $a = (a^1, a^2, \dots, a^N) \sim \pi(a|s)$ can be written as:

$$\begin{aligned}
\mathcal{H}(\pi(a|s)) &= \int_a -\pi(a|s) \log(\pi(a|s)) da \\
&= \int_a -\prod_{j=1}^n \pi_j(a^j|s) \log\left(\prod_{i=1}^n \pi_i(a^i|s)\right) da \\
&= \int_a -\prod_{j=1}^n \pi_j(a^j|s) \sum_{i=1}^n \log(\pi_i(a^i|s)) da \\
&= \sum_{i=1}^n \int_{a^1, \dots, a^N} -\prod_{j=1}^n \pi_j(a^j|s) \log(\pi_i(a^i|s)) da^1 \dots da^N \\
&= \sum_{i=1}^n \int_{a^i} -\pi_i(a^i|s) \log(\pi_i(a^i|s)) da^i \\
&= \sum_{i=1}^n \mathcal{H}(\pi_i(a^i|s)).
\end{aligned} \tag{16}$$

It means that the entropy of the joint policy can be split as the summation of the independent policy. Moreover, we calculate the evidence lower bound of a single-agent policy, which is the same as [8] that (here we renotate that $a^i = a_0^i$ and notate the policy of agent i as π_{θ_i} to involve the terminal timestep for the reverse diffusion process) and the corresponding forward process as π :

$$\mathcal{H}(\pi(a_0^i|s)) = \int_{a_0^i} -\pi_{\theta_i}(a_0^i|s) \log(\pi_{\theta_i}(a_0^i|s)) da_0^i = \mathbb{E}_{\pi_{\theta_i}}[-\log(\pi_{\theta_i}(a_0^i|s))] \tag{17}$$

Notice that $\pi_{\theta_i}(a_{0:H}^i|s) = \pi_{\theta_i}(a_0^i|s)\pi_{\theta_i}(a_{1:H}^i|a_0^i, s)$, so we replace $\pi_{\theta_i}(a_0^i|s) = \frac{\pi_{\theta_i}(a_{0:H}^i|s)}{\pi_{\theta_i}(a_{1:H}^i|a_0^i, s)}$ such that:

$$\begin{aligned}
\mathbb{E}_{\pi_{\theta_i}}[-\log(\pi_{\theta_i}(a_0^i|s))] &= \mathbb{E}_{\pi_{\theta_i}} \left[-\log \left(\frac{\pi_{\theta_i}(a_{0:H}^i|s)}{\pi_{\theta_i}(a_{1:H}^i|a_0^i, s)} \right) \right] \\
&= \mathbb{E}_{\pi_{\theta_i}} \left[\log \left(\frac{\pi_{\theta_i}(a_{1:H}^i|a_0^i, s)}{\pi_{\theta_i}(a_{0:H}^i|s)} \right) \right] \\
&\geq \mathbb{E}_{\pi_{\theta_i}} \left[\log \left(\frac{\pi(a_{1:H}^i|a_0^i, s)}{\pi_{\theta_i}(a_{0:H}^i|s)} \right) \right] = l_{\pi_{\theta_i}}(a_0^i|s).
\end{aligned} \tag{18}$$

The final inequality is due to the fact that:

$$\begin{aligned}
\mathbb{E}_{\pi_{\theta_i}}[\log(\pi_{\theta_i}(a_{1:H}^i|a_0^i, s))] &= \mathbb{E}_{\pi_{\theta_i}}[\log(\pi_{\theta_i}(a_{1:H}^i|a_0^i, s)) - \log(\pi(a_{1:H}^i|a_0^i, s)) + \log(\pi(a_{1:H}^i|a_0^i, s))] \\
&= \mathbb{KL}(\pi_{\theta_i}(a_{1:H}^i|a_0^i, s) \parallel \pi(a_{1:H}^i|a_0^i, s)) + \mathbb{E}_{\pi_{\theta_i}}[\log(\pi(a_{1:H}^i|a_0^i, s))] \\
&\geq \mathbb{E}_{\pi_{\theta_i}}[\log(\pi(a_{1:H}^i|a_0^i, s))].
\end{aligned} \tag{19}$$

It means that $\mathbb{E}_{\pi_{\theta_i}}[\log(\pi_{\theta_i}(a_{1:H}^i|a_0^i, s))] \geq \mathbb{E}_{\pi_{\theta_i}}[\log(\pi(a_{1:H}^i|a_0^i, s))]$ due to the non-negativity of the KL divergence. Combine Eq. (16), Eq. (18) and Eq. (19), we complete the proof.

C Derivation of the Synchronized Policy Objective

In this section, we present the background and motivation for our synchronized policy objective. We define our objective function as: $J(\boldsymbol{\pi}_{\theta}(\cdot|s)) := \mathbb{E}_{\boldsymbol{\pi}_{\theta}} \left[\sum_{t=0}^{\infty} \sum_{i=1}^N \gamma^t (r_t^i + \alpha l_{\pi_{\theta_i}}(a_t^i, s_t)) \right]$. Incorporating a scaled maximum entropy regularizer, we define the corresponding value function for a joint state-action pair as follows:

$$Q^{\pi}(s_t, a_t^0) = \sum_{i=1}^N r_t^i + \sum_{l=1}^{\infty} \gamma^l \mathbb{E}_{\rho_{\pi}} \left[\sum_{i=1}^N (r_{t+l}^i + \alpha l_{\pi_i}(a_{t+l}^i, s_{t+l})) \right]. \quad (20)$$

This definition aligns with Eq. (17) in [8] for joint states and actions. Given a concrete policy π , the iterative policy optimization aims to minimize the KL divergence between the policy and the exponential soft Q-values:

$$\pi^{k+1} = \arg \min_{\pi} D_{\text{KL}} \left(\pi(\cdot|s) \left\| \frac{\exp(\frac{1}{\alpha} Q^{\pi^k}(s, \cdot))}{Z(s)} \right. \right), \quad (21)$$

which corresponds to Eq. (5) in [41]. Since the exact likelihood of the diffusion policy is intractable, we upper bound the KL divergence as (which builds upon Eq. (20) in [8]):

$$D_{\text{KL}} \left(\pi_{\theta}(\cdot|s) \left\| \frac{\exp(\frac{1}{\alpha} Q_{\phi}(s, \cdot))}{Z(s)} \right. \right) \leq D_{\text{KL}}(\pi_{\theta}(a_{0:H}|s) \|\pi(a_{0:H}|s)). \quad (22)$$

The trajectory distributions are factorized as:

$$\begin{aligned} \pi_{\theta}(a_{0:H}|s) &= \prod_{i=1}^N \pi_{\theta_i}(a_{0:H}^i|s) = \prod_{i=1}^N \pi_{\theta_i}(a_{i:H}^i|s) \prod_{h=1}^H \pi_{\theta_i}(a_{h-1}^i|a_h^i, s), \\ \pi(a_{0:H}|s) &= \pi(a_0|s) \prod_{h=0}^{H-1} \pi(a_{h+1}|a_h, s) = \pi(a_0|s) \prod_{h=0}^{H-1} \prod_{i=1}^N \pi(a_{h+1}^i|a_h^i, s). \end{aligned} \quad (23)$$

Here, $\pi_{\theta}(a_{0:H}|s)$ represents the probability that the action is sampled via the reverse diffusion process for each individual agent, corresponding to Eq. (13) and Eq. (14) in [8]. The target policy is defined as a forward diffusion process, where $\pi(a_0|s) = \frac{1}{Z(s)} \exp(\frac{1}{\alpha} Q_{\phi}(s, a_0))$ is the target distribution and $\pi(a_{h+1}^i|a_h^i, s)$ corresponds to the forward diffusion term. By substituting these terms into the KL divergence objective, we obtain:

$$\begin{aligned}
\mathcal{L}(\theta) &= D_{\text{KL}}(\pi_{\theta}(a_{0:H}|s) \parallel \pi(a_{0:H}|s)) \\
&= \mathbb{E} \left[\log \left(\frac{\pi_{\theta}(a_{0:H}|s)}{\pi(a_{0:H}|s)} \right) \right] \\
&= \mathbb{E} \left[\log \left(\frac{\prod_{i=1}^N \pi_{\theta_i}(a_H^i|s) \prod_{h=1}^H \pi_{\theta_i}(a_{h-1}^i|a_h^i, s)}{\pi(a_0|s) \prod_{h=0}^{H-1} \prod_{i=1}^N \pi(a_{h+1}^i|a_h^i, s)} \right) \right] \\
&= \mathbb{E} \left[\sum_{i=1}^N \log \pi_{\theta_i}(a_H^i|s) - \frac{1}{\alpha} Q_{\phi}(s, a_0) + \sum_{i=1}^N \sum_{h=1}^H \log \frac{\pi_{\theta_i}(a_{h-1}^i|a_h^i, s)}{\pi_i(a_h^i|a_{h-1}^i, s)} \right] + \log Z(s).
\end{aligned} \tag{24}$$

Note that the target policy is defined based on the joint distributional value $Q_{\phi}(s, a) = \mathbb{E}[Z_{\phi}(s, a)]$, implying that the loss function is shared across all agents. Crucially, this design choice is pivotal for coordination: while we employ a factorized entropy lower bound for computational tractability in Eq. (16), the multi-agent coordination is strictly enforced by the global guidance of this centralized distributional critic $Z_{\phi}(s, a)$. In contrast to independent learning methods, the joint critic explicitly models the complex, multi-modal correlations of agent interactions and backpropagates a unified gradient signal, thereby synchronizing the decentralized diffusion processes towards a coherent joint equilibrium.

Given this strong coordination signal, while applying value factorization techniques could theoretically enable distributed policy optimization by assigning appropriate credits to different agents, our empirical results suggest that these techniques are insufficient to guide the policy toward optimal behaviors in this setting compared to our joint critic approach. Furthermore, leveraging an off-policy paradigm, our framework allows for repeated sampling from the replay buffer, thereby maximizing data utility and significantly outperforming on-policy counterparts in sample efficiency.

D Details about the Experiments

D.1 Experimental Setup: Environments

We evaluate our algorithm and baselines on two standard benchmarks: the Multi-Agent Particle Environments (MPE) [37]¹ and Multi-Agent MuJoCo (MAMuJoCo) [47]². Within the MPE domain, we select *Cooperative Navigation* and *Physical Deception* as representative scenarios. In Cooperative Navigation shown as Figure 7a, agents must coordinate to occupy landmarks while avoiding collisions. In Physical Deception shown as Figure 7b, agents collaborate to reach a target landmark while concealing its identity from an adversary.

In the Multi-Agent MuJoCo (MAMuJoCo) domain, we evaluate our method across a diverse set of locomotion scenarios, including *Ant* in Figure 7c, *HalfCheetah* in Figure 7d, *Walker2d* in Figure 7e, and *Swimmer* in Figure 7f. In these tasks, the original high-dimensional action space of a single robot is partitioned among multiple decentralized agents. This partitioning necessitates complex

¹<https://pettingzoo.farama.org/environments/mpe/>

²<https://robotics.farama.org/envs/MaMuJoCo/>

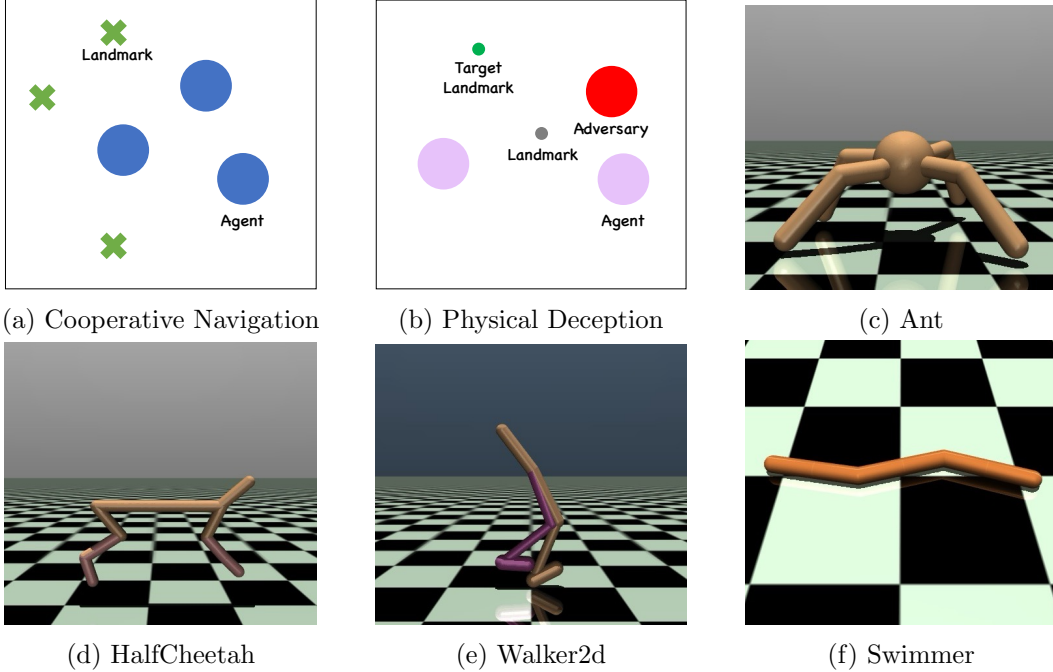


Figure 7: Multi-agent particle environments (MPE) and Multi-agent HalfCheetah task in MuJoCo Environment (MAMuJoCo).

coordination, as agents must infer the intentions of others and align their local policies to achieve stable and rapid global locomotion. The specific characteristics of each environment are detailed below:

Ant (2×4 , $2 \times 4d$, 4×2) A 3D quadrupedal robot with high-dimensional state-action spaces. Different from planar tasks, the Ant requires agents to maintain balance in three dimensions while coordinating four multi-joint legs. The challenge lies in synchronizing independent limb movements to generate forward velocity without toppling the robot.

HalfCheetah (2×3 , 6×1) A planar biped designed for high-speed running. In multi-agent configurations, the primary difficulty is synthesizing a coherent, rhythmic gait from partitioned actuation (e.g., separate agents for thighs and feet). Agents must maximize forward momentum through emergent cooperation without the strict balance constraints.

Walker2d A bipedal walker that introduces significant stability constraints. In contrast to the HalfCheetah, the Walker2d must maintain an upright torso to avoid falling. Agents controlling different leg segments face a difficult credit assignment problem, as they must balance the trade-off between generating forward thrust and actively stabilizing the robot’s pitch.

Swimmer Locomotion in a viscous fluid governed by fluid dynamics rather than ground reaction forces. Agents must coordinate to produce undulatory, snake-like motion. The task requires precise temporal synchronization along the kinematic chain to leverage fluid friction effectively, as uncoordinated actions result in negligible displacement.

The fundamental distinction between the standard MuJoCo benchmark and MAMuJoCo lies in the partitioning of the control authority. In the single-agent setting, a monolithic policy governs the entire kinematic chain, implicitly handling the coordination between joints through centralized optimization. In contrast, MAMuJoCo transforms these tasks into decentralized coordination problems where the action space is split among independent agents. This introduces significant challenges: (1) *Physical Coupling*: due to the rigid-body dynamics, an action taken by one agent instantaneously alters the state dynamics experienced by others, creating a highly non-stationary environment; (2) *Implicit Coordination*: agents must achieve global synchronization (e.g., a stable gait) purely through local observations and rewards, without explicit communication channels. Success in this domain thus demonstrates an algorithm’s capability to solve complex credit assignment problems in high-dimensional continuous control tasks.

Table 1: Hyperparameters in the MPE and MAMuJoCo environment for all tasks.

Name of the Hyperparameter	Value
Warmup Timesteps	60000
Timesteps to Start Learning L_{init}	5000
Policy Soft Update ρ	0.0
Discount Factor γ	0.99
Policy Delay d_l	3
Batch Size	256
Buffer Size of \mathcal{D}	1000000
Initial Entropy Coefficient Term α	1.0
Target Entropy $\mathcal{H}_{\text{target}}$	$4\dim(\mathcal{A})$
Number of Atoms for Distributional Q-Learning N_{atoms}	100
Coefficient Term for Distributional Q-Learning Regularization ξ	0.005
Batch Normalization Momentum	0.99
Batch Normalization Warmup Timesteps	100000
Optimizer	Adam
Adam β_1	0.5
Adam β_2	0.999
Gradient Clip Norm	1.0
Diffusion Denoise Steps H	8

D.2 Experimental Setup: Network Structures and Hyperparameters

For the critic, we employ a Multi-Layer Perceptron (MLP) to model the distributional Q-function. Following the CrossQ technique [6], we concatenate the state-action pairs and normalize them via

Table 2: Hyperparameters in the MPE and MAMuJoCo environment for all tasks including the learning rate for the actor and critic, and the maximum value V_{\max} for distribution Q-Learning.

Task	Learning Rate	Maximum Value V_{\max}
Cooperative Navigation 3 Agents	3.5×10^{-5}	200
Cooperative Navigation 4 Agents	2.5×10^{-5}	200
Physical Deception 2 Agents	5.0×10^{-6}	200
Ant 2×4	7.0×10^{-6}	1200
Ant $2 \times 4d$	2.0×10^{-5}	5000
Ant 4×2	5.0×10^{-6}	3000
HalfCheetah 2×3	1.0×10^{-4}	20000
HalfCheetah 6×1	1.0×10^{-3}	3000
Walker2d 2×3	5.0×10^{-6}	50000
Swimmer 2×1	2.0×10^{-5}	400

a Batch Normalization layer before feeding them into the MLP. The network consists of two hidden layers with 2048 units each, utilizing ReLU activations and Batch Normalization. The final output is processed via a softmax function to generate the probability distribution over the atoms. The support of the distribution is defined over $[V_{\min}, V_{\max}]$, where $V_{\min} = -V_{\max}$ for all tasks.

For the actor, we utilize a diffusion-based policy parameterized by a noise prediction network $f_{\theta_i}(a_t^i, s, t)$. This network is implemented as a 3-layer MLP with GeLU activations and a hidden dimension of 256. The input consists of the concatenated state, noisy action, and a 256-dimensional Fourier timestep embedding. We employ a cosine noise schedule with $\beta_{\min} = 10^{-3}$ and $\beta_{\max} = 0.9999$. The number of diffusion steps H is set to 8 for both training and inference. Similar to the critic, the input vector undergoes Batch Normalization prior to entering the MLP layers. We emphasize that while our centralized distributional critic adopts the CrossQ architecture to forego the target Q-network, we explicitly retain the target policy network. This design ensures training stability during data collection and stabilizes the joint optimization of the critic and actor. Crucially, sampling next-step actions from a slowly updating target policy mitigates the high variance arising from the compounded stochasticity of interacting diffusion agents, thereby preventing divergence in value estimation.

To facilitate full reproducibility, we provide a detailed breakdown of the experimental configurations. Table 1 summarizes the common hyperparameters applied uniformly across all tasks, such as network architecture and optimizer settings. In contrast, Table 2 details the task-specific hyperparameters, including learning rates and distributional value limits, which are tailored to each environment. All reported experiments were conducted using 5 independent random seeds to ensure statistical reliability.

D.3 Additional Experimental Results and Visualization

To rigorously evaluate the asymptotic performance and robustness of our approach, we conduct extensive experiments. To highlight OMAD’s efficiency, the training horizon for baselines is extended to 1×10^7 steps to guarantee convergence. In contrast, OMAD requires only within just 3×10^6 steps (except for HalfCheetah 6×1 , which uses 1×10^6). As detailed in Table 3, OMAD consistently outperforms all baselines despite their significantly longer training horizons. We report the maximum average episode returns over 5 random seeds, highlighting the optimal performance in bold. These results show that OMAD achieves state-of-the-art performance across nearly all MPE and MAMuJoCo tasks with low variance. This comprehensive evaluation underscores that OMAD not only excels in sample efficiency but also delivers superior final performance, validating its effectiveness for long-horizon multi-agent control.

These comparative results also offer implicit insights into the structural determinants of multi-agent coordination. Notably, the diffusion-based baselines (MADPMD and MASDAC) were implemented using a centralized training and centralized execution paradigm to incorporate them into the multi-agent environments. While this approach theoretically maximizes coordination by circumventing the limitations of distributed policies, their suboptimal performance underscores that merely incorporating expressive diffusion policies is insufficient without a robust value estimation mechanism and efficient design of the diffusion policy architecture. We argue that the advanced distributional critic alone is insufficient, as unimodal Gaussian policies inevitably suffer from sub-optimal mean-seeking behavior in multi-modal multi-agent landscapes. OMAD’s superior performance stems from the synergy between the distributional critic and the expressive diffusion policy, which naturally models multi-modality to fully leverage the critic’s rich guidance.

Furthermore, regarding the policy structure, while OMAD employs an SDE-based formulation to ensure sustained stochasticity, identifying network architectures that maximize the trade-off between training efficiency and control performance remains an important open question. Additionally, the theoretical implications of the ELBO approximation error warrant further scrutiny. While the intractable likelihood of diffusion models precludes a precise quantification of the variational approximation gap during training, this error theoretically vanishes as the learned policy converges to the optimal target distribution. Consequently, deriving tighter lower bounds to mitigate potential bias remains a valuable direction for theoretical refinement.

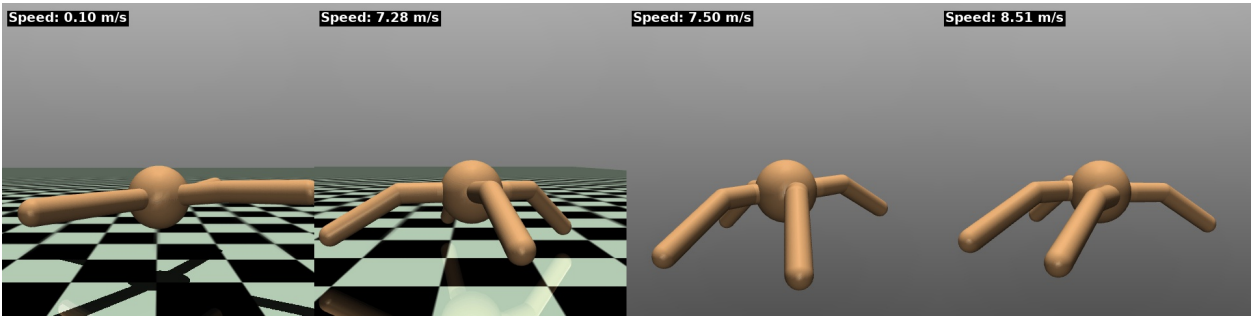
Table 3: Quantitative comparison of asymptotic performance on MPE and MAMuJoCo benchmarks. We report the maximum average episode returns and the standard deviation over 5 random seeds. Notably, OMAD achieves state-of-the-art results despite being trained for significantly fewer timesteps (3×10^6) compared to the extended horizon of baselines (1×10^7), demonstrating exceptional sample efficiency. An exception is HalfCheetah 6×1 , where diffusion models were evaluated at 1×10^6 steps. Bold indicates optimal performance (within 1% gap).

Task	HATD3	HASAC	MADPMD	MASDAC	OMAD(Ours)
Cooperative Navigation $N = 3$	-26.2 ± 3.5	-25.1 ± 1.3	-29.4 ± 1.6	-41.0 ± 1.1	-23.9 ± 1.1
Cooperative Navigation $N = 4$	-63.0 ± 2.2	-65.6 ± 3.5	-85.0 ± 3.8	-84.6 ± 3.1	-57.9 ± 0.8
Physical Deception $N = 2$	43.0 ± 3.6	45.4 ± 3.1	36.9 ± 4.5	33.1 ± 5.1	45.1 ± 4.1
Ant 2×4	6151.9 ± 408.9	6980.4 ± 458.5	7042.7 ± 379.8	7266.2 ± 431.5	7517.0 ± 279.2
Ant $2 \times 4d$	4992.1 ± 595.2	4941.9 ± 320.0	6672.5 ± 467.5	6936.2 ± 309.7	7449.3 ± 169.3
Ant 4×2	5911.2 ± 254.0	6597.1 ± 418.7	7139.9 ± 462.1	6198.5 ± 1012.1	7403.7 ± 41.7
HalfCheetah 2×3	8732.6 ± 413.6	8835.7 ± 356.3	10305.5 ± 735.9	10540.7 ± 963.8	14368.5 ± 1166.0
HalfCheetah 6×1	8453.7 ± 503.4	8714.3 ± 424.6	10402.8 ± 622.4	10049.9 ± 751.4	11044.3 ± 249.6
Walker2d 2×3	6248.6 ± 622.3	6753.5 ± 436.2	6112.8 ± 269.3	8154.4 ± 322.5	8180.4 ± 803.5
Swimmer 2×1	98.5 ± 52.3	134.2 ± 23.3	136.8 ± 7.6	149.3 ± 12.6	162.0 ± 22.5

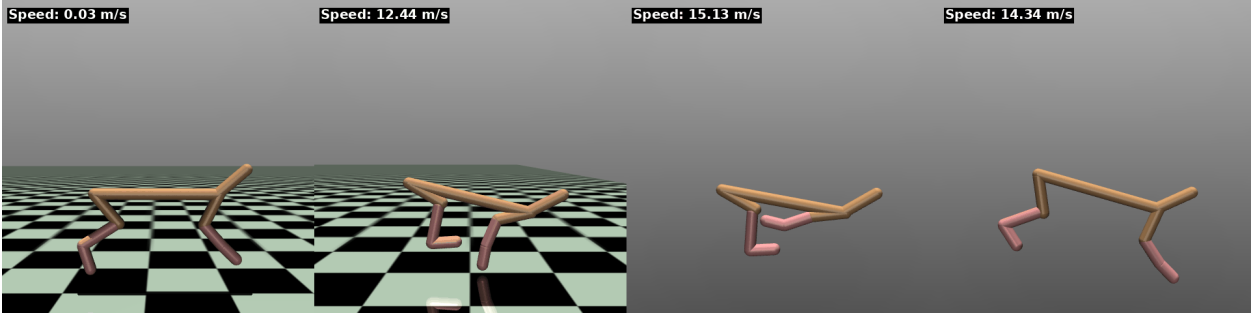
Moreover, in terms of computational cost, although hardware variations introduce some noise in wall-clock measurements, OMAD generally exhibits superior performance compared to HASAC and HATD3 within equivalent timeframes. Nevertheless, developing techniques to further optimize the wall-clock training efficiency of diffusion-based agents remains a vital direction for enhancing the scalability of this framework.

It is worth noting that this work explicitly focuses on efficient online multi-agent coordination within the continuous control domain, as validated by extensive experiments on representative benchmarks. Extending the framework to discrete action spaces (e.g., via discrete diffusion) presents a promising avenue for future research to further broaden its applicability.

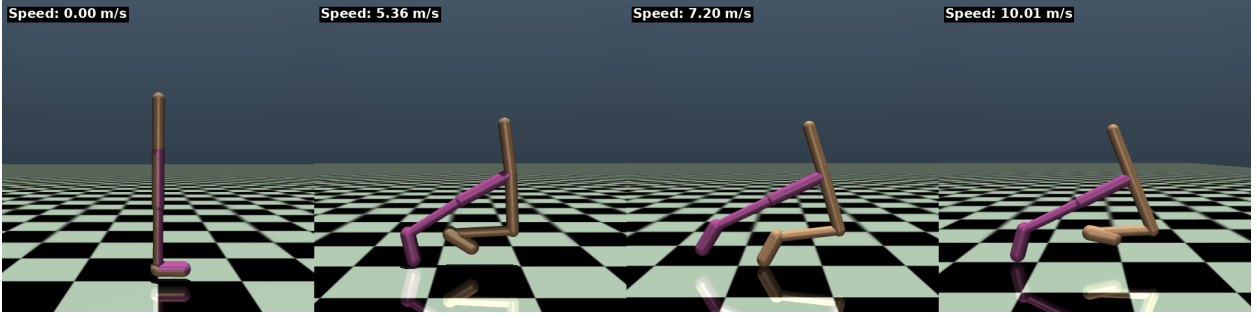
To further validate the effectiveness of OMAD beyond numerical metrics, we provide a qualitative visualization of the learned behaviors in Figure 8. The figure displays the temporal evolution of agent policies across four distinct MAMuJoCo tasks (Ant 4×2 , HalfCheetah 6×1 , Walker2d 2×3 , and Swimmer 2×1 as the representative tasks) at timesteps $t \in \{1, 100, 250, 500\}$. As observed, the agents rapidly transition from initial states to stable, high-velocity locomotion. Notably, in complex scenarios such as Ant 4×2 and HalfCheetah 6×1 , the physically decoupled agents exhibit remarkable inter-agent coordination, effectively synchronizing their joint movements to maintain balance and maximize forward momentum without conflicts. The high episode returns annotated in



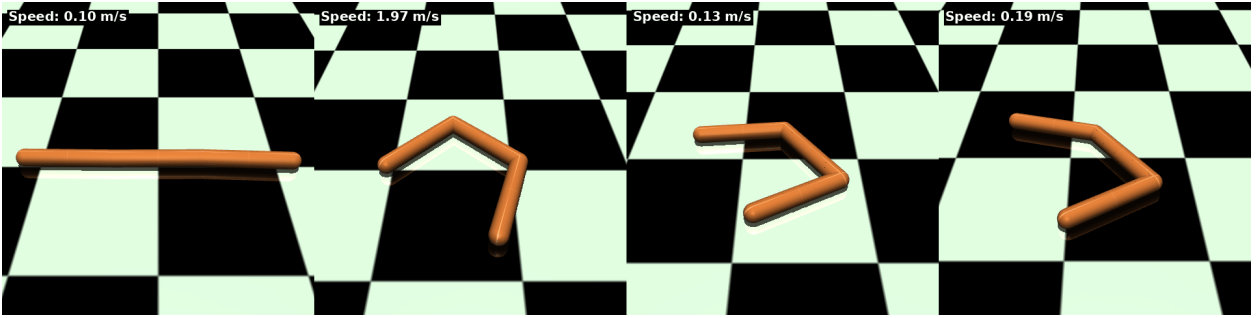
(a) Ant 4×2 Return = 7521.9



(b) HalfCheetah 6×1 Return = 12499.8



(c) Walker2d 2×3 Return = 10182.4



(d) Swimmer 2×1 Return = 156.6

Figure 8: Visualization of learned diffusion policies across four distinct MAMuJoCo tasks. We display snapshots of the agents at timesteps $t \in \{1, 100, 250, 500\}$ with the instantaneous velocity, demonstrating the stable and coordinated behaviors achieved by our OMAD algorithm.

the figure (e.g., 12499.8 for HalfCheetah and 7521.9 for Ant) significantly surpass the performance of competing multi-agent baselines reported in Table 3. These visual results confirm that OMAD not only optimizes for scalar rewards but also successfully masters the intricate dynamics required for robust and cooperative multi-agent control.